Journal of Alloys and Compounds, 207/208 (1994) 444–448
JALCOM 3037

The oxidation state of cerium in Ce_2MoO_6

Mark R. Antonio, J. Simon Xue and L. Soderholm
Argonne National Laboratory, Chemistry Division, 9700 South Cass Avenue, Argonne, IL 60439-4831 (USA)

Abstract

Synchrotron radiation was used to determine the oxidation state of cerium in Ce_2MoO_6 through Ce L-edge X-ray absorption fine structure (XAFS). The results from this direct spectroscopic investigation reveal that, to the level of sensitivity of the technique, cerium is trivalent in Ce_2MoO_6. Magnetic susceptibility data over the temperature range 10–300 K do not follow the Curie Law and, therefore, cannot be used to support any assignment of valence. The possible origins of the unique structure and colour of the RE = Ce analogue of the RE_2MoO_6 series are discussed.

1. Introduction

Rare earth (RE) metalates with the composition $RE_2O_3 \cdot MO_3$ (RE = La–Nd, Sm–Lu; M = Mo, W) crystallize in five different structural modifications [1–4]. In nearly all of these compounds, the assignments of formal oxidation states to the rare earth and transition metal cations are straightforward (*i.e.* RE^{III} and M^{VI}). These materials are all poor conductors, and assume the color of the trivalent rare earth ion, as expected because the M^{VI}–O sublattice has no carriers. An exception occurs for Ce_2MoO_6, which is black. This color has been attributed to an unusual, mixed distribution of cerium and molybdenum valences, Ce^{III}-$Ce^{IV}Mo^{V}O_6$ [4]. Previously reported magnetic and spectroscopic studies have been interpreted in support of this cation valence distribution [5].

As part of our studies of binary cerium sesquioxides ($Ce_2O_3 \cdot nMO_3$ for $n = 1$, 2, 3 and M ≡ Mo, Te, W, U), we have investigated the chemical state of cerium in Ce_2MoO_6. Ce L-edge XAFS (X-ray absorption fine structure) was used as a direct probe of the valence and coordination of cerium in Ce_2MoO_6. The results of these Ce XANES (X-ray absorption near edge structure) and EXAFS (extended X-ray absorption fine structure) as well as magnetic susceptibility measurements are described.

2. Experimental details

Ce_2MoO_6, in the form of a black powder, was prepared according to the method of Brixner *et al.* [4]. X-Ray diffraction data were in agreement with previous reports [3–5], except that for select preparations, there were several extra, very weak reflections attributable to a low symmetry cell. Refinement of the cubic cell parameter using the *Fm3m* reflections resulted in a lattice constant similar to that previously reported [4]. A Quantum Design SQUID magnetometer was used to obtain magnetic data as a function of field and temperature. A field run to 2 T showed a linear magnetization with all field strengths. Susceptibility data were acquired in an applied field of 0.5 T for a 35.31-mg powder sample.

Ce L_3-, L_2- and L_1-edge (5723, 6164, 6548 eV, respectively) XAFS were collected at ambient temperature on beam line X-23A2 at the National Synchrotron Light Source with a Si⟨3 1 1⟩ double crystal monochromator. To obtain accurate edge resonance intensities and positions, the XAFS was detected by use of the electron-yield technique [6]. The vertical slit was optimized (1 mm) to provide a total energy bandwidth (the quadratic sum of the monochromator rocking curve width ($2\delta E = 0.3$ eV) and the X-ray beam divergence ($\Delta E = 0.7$ eV)) of 0.8 eV at 6000 eV. With this configuration, the instrumental resolution ($\Gamma = 0.8$ eV) is *ca.* 4.4 times smaller than the natural linewidths (*ca.* 3.5 eV [7]) of the Ce L_3 and L_2 core holes. Hence, the XAFS shown here is not obviously broadened (< 3%) by either instrumental effects or sample thickness effects. The three L-edge regions were scanned independently under the same experimental conditions with a step size of 0.25 eV/pt ($L_{2,3}$-edges) and 0.4 eV/pt (L_1 edge). The scan-to-scan energy calibration was maintained to ±0.2 eV. Although short, the range of the Ce L_3-edge

0925-8388/94/$07.00 © 1994 Elsevier Science S.A. All rights reserved
SSDI 0925-8388(93)03037-J

EXAFS ($\Delta k = 10$ Å^{-1}) was sufficient to provide metrical information about the cerium coordination environment. The analyses of the XANES and EXAFS were performed according to conventional methods [8].

3. Results and discussion

3.1. Magnetic susceptibility

The magnetic susceptibility as a function of temperature is shown as a Curie plot in Fig. 1. The data show marked curvature as plotted, indicating that the Curie–Weiss law is not obeyed over this temperature range, 10–300 K. Instead, a plot of χT versus T, as shown in the inset of Fig. 1, is linear over a considerable temperature range, indicating that there is a large temperature independent (TIP) contribution to the measured susceptibility. The large value of the measured TIP is somewhat surprising because Ce_2MoO_6 is not a good metal [3] and therefore the TIP does not arise from conduction electrons. However, it may be interpreted as evidence of a second order crystal field contribution to the measured susceptibility. Unfortunately, the magnetic behaviors of both Ce and Mo may both be complex [9]. Even when they have stable, well defined oxidation states, both Ce and Mo can give rise to a range of magnetic behaviours, dependent on their degree of hybridization and the symmetry of their environment, as well as the direct effect of the crystal field on the number and distribution of low-lying energy states.

3.2. XANES

Our initial experiments for valence determination focus on cerium instead of molybdenum because Ce L-edge XANES is much better resolved than Mo K-edge XANES. In general, high resolution XANES is more readily obtainable at low than at high energies for two reasons: (1) the extrinsic spectral broadening due to the optical system (*i.e.* the X-ray source divergence and the monochromator crystal rocking curve width) decreases with decreasing X-ray energy, and; (2) the intrinsic spectral broadening, caused by the natural lifetime of the excited core state, is smaller for the shallow L shells than the deep K shell. At the Ce L_3-edge energy (5723 eV), the experimental broadening is some ten times less than that at the Mo K-edge energy (20 000 eV), and the lifetime broadening of the Ce L_3-edge core hole (3.48 eV [7]) is about 3/4 of that for the Mo K-edge core hole (4.52 eV [7]). Although Mo K-edge XANES inflection point energies have been shown to correlate with molybdenum oxidation states [10,11], Mo and Ce valence is much more readily and precisely determined from L-edge XANES [12,13]. In fact, the use of Ce L_3-, L_2- and L_1-edge XANES permits a clear distinction between trivalent and quadrivalent cerium [14–16].

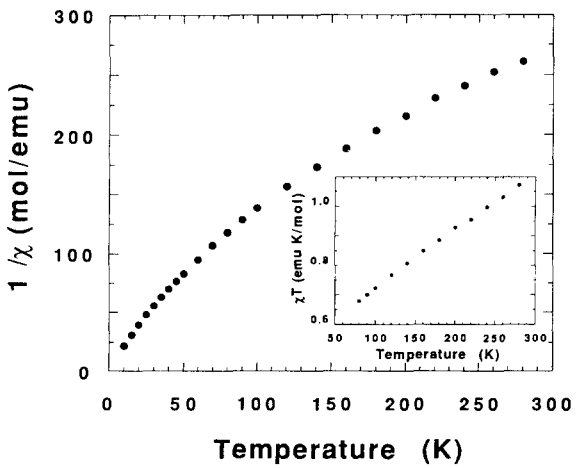

Fig. 1. Magnetic susceptibility of Ce_2MoO_6 as a function of temperature in an applied field of 0.5 T.

The normalized Ce L_3- and L_1-edge XANES of Ce_2MoO_6 and CeO_2 are displayed in Fig. 2. The intense single resonance at 5722.2 eV in the L_3-edge XANES of Ce_2MoO_6 is typical of trivalent cerium [13–16]. This resonance is due to an electronic (dipole) transition from the Ce $2p_{3/2}$ initial state to the 5d orbital manifold. For formally quadrivalent cerium compounds, such as CeO_2, the Ce L_3-edge XANES exhibits two well-resolved resonances. The peak-to-peak separation for $Ce^{IV}O_2$ is 7.7 eV and, most important, the first peak of the characteristic cerium(IV) doublet is some 3.5–4.0 eV higher than the single L_3-edge resonance typical of cerium(III). The Ce L_2-edge XANES (not shown) exhibit identical characteristics. The position (6563.6 eV) of the L_1-edge peak of Ce_2MoO_6 with respect to that of *ca.* 6562 eV for Ce^{III} compounds and *ca.* 6574 eV for Ce^{IV} compounds [16] confirms the presence of Ce^{III} cations in Ce_2MoO_6. The results of curve fitting analyses of the Ce L_3-edge XANES for Ce_2MoO_6 are compared (Table 1) with those for several compounds with well-defined Ce oxidation states. The parameters of the Ce_2MoO_6 XANES are remarkably similar to those of the cerium(III) compounds, particularly $CeTiO_3$. The large Lorentz peak areas (21.2–22.3) and heights (4.0), as well as the narrow widths (3.4–3.6 eV) observed for $Ce_2(C_2O_4)_3 \cdot nH_2O$ and $Ce(NO_3)_3 \cdot nH_2O$, are characteristic of ionic Ce compounds with localized (*i.e.* atomic-like) empty 5d orbitals. In contrast, for Ce_2MoO_6, the small Lorentz peak area (18.9) and height (2.2) as well as the large width (5.4 eV) suggest a covalent Ce^{III} environment in which the Ce 5d orbitals are hybridized with the oxygen 2p orbitals.

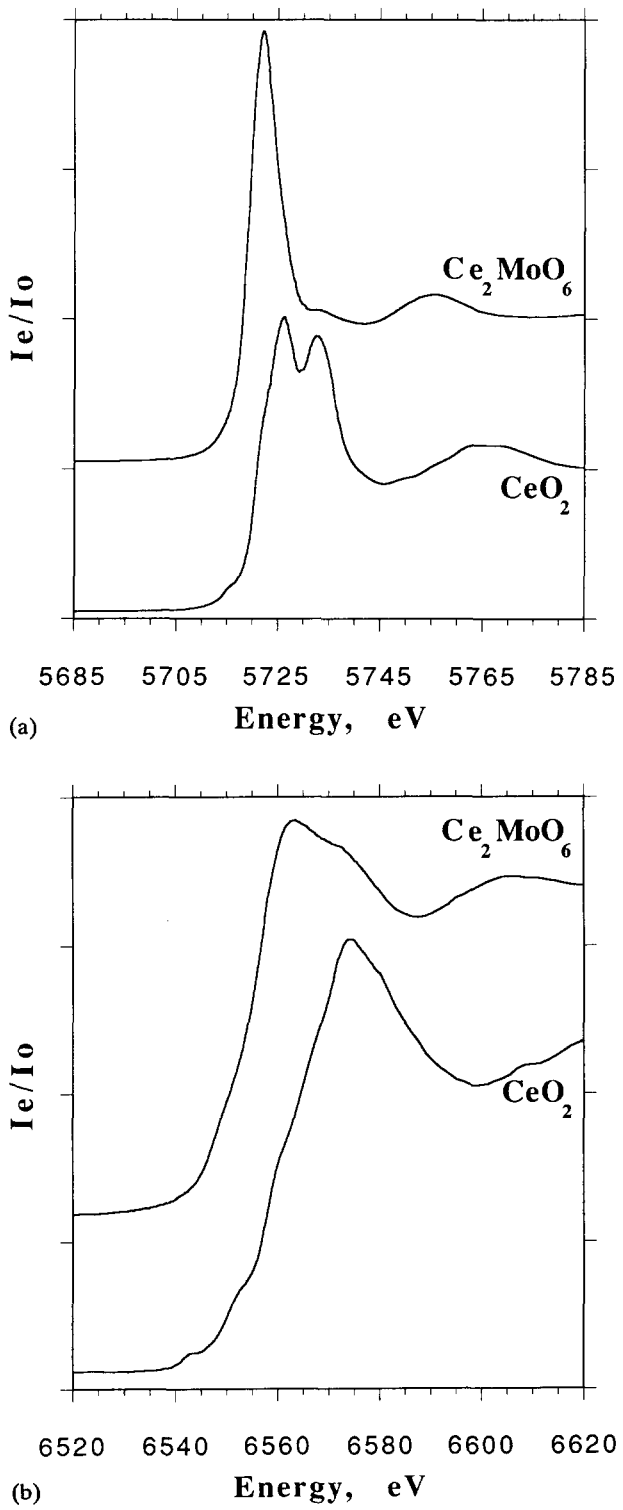

Fig. 2. Cerium L-edge XANES for Ce_2MoO_6 and CeO_2 obtained through electron-yield at ambient temperature: (a) L_3-edge; (b) L_1-edge.

3.3. EXAFS

Although the range of Ce L_3-edge EXAFS is restricted to *ca.* 400 eV (10 $Å^{-1}$) by the onset of the Ce L_2-edge, the data are of sufficient length and quality to provide metrical information about the Ce coordination. The $k^3\chi(k)$ EXAFS and the corresponding Fourier transform (FT) data are shown in Figs. 3(a) and (b), respectively. The two peaks in the FT data at 1.77 and 2.36 Å (before phase shift correction) are due to backscattering by oxygen atoms and the distant peak at *ca.* 3.5 Å is due to Ce–M (M = Ce, Mo) backscattering. Curve fitting analysis of the Fourier filtered ($\Delta r = 2.13$ Å) Ce–O EXAFS reveals 4 ± 1 O atoms at 2.43(3) Å and 4 ± 1 O atoms at 2.70(3) Å about cerium. The average Ce–O interatomic distance for Ce_2MoO_6 (2.57(4) Å) is typical of Ce^{III}–O distances and serves to further substantiate the XANES results (*vide supra*). For comparison, the average Ce–O distances in $Ce^{III}NbO_4$ and $Ce^{III}TaO_4$ are 2.480 and 2.520 Å, respectively [17]; for A–Ce_2O_3, the average Ce–O distance is 2.505 Å [18]. All of these distances, including those for Ce_2MoO_6, are significantly

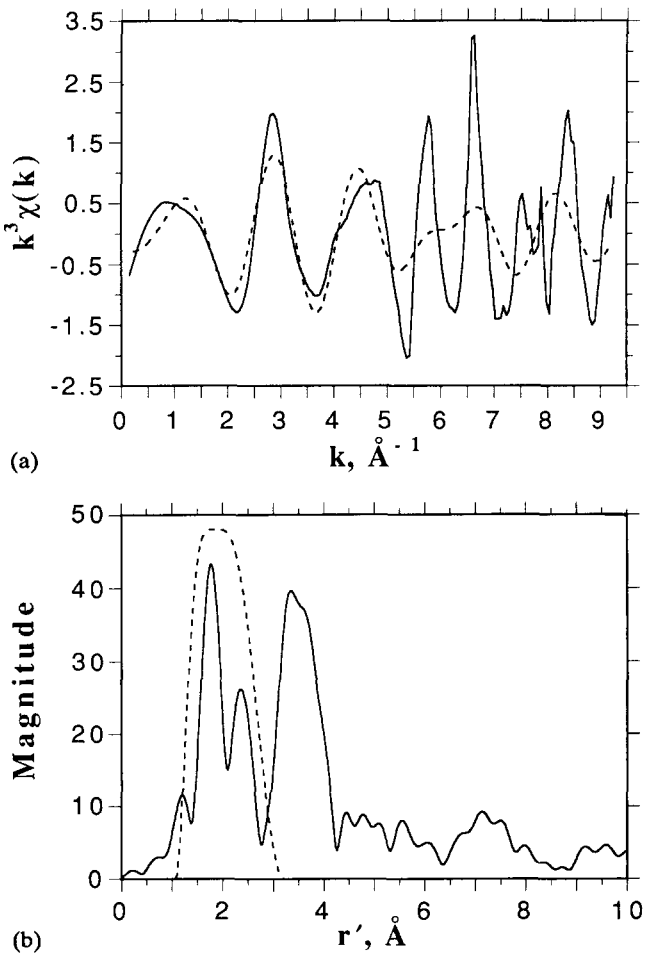

Fig. 3. (a) Cerium L_3-edge $k^3\chi(k)$ EXAFS of Ce_2MoO_6 (solid line) and the Fourier filtered Ce–O EXAFS (dashed line). The background absorption of the primary experimental data (I_e/I_0 versus eV) was approximated by use of three sections of cubic splines ($\Delta k = 3.03$ $Å^{-1}$) fit from 5726 (E_0) to 6055 eV. (b) Fourier transform magnitude (solid line) of the $k^3\chi(k)$ EXAFS of Ce_2MoO_6 and the filtering window (dashed line, $\Delta r = 2.13$ Å).

TABLE 1. Areas (A), heights (H), widths (W, eV), and positions (E, eV) of the $2p_{3/2} \rightarrow 5d$ resonance and continuum states in the normalized, electron-yield Ce L_3-edge XANES as obtained by curve fitting with Lorentz and arctangent functions, respectively, convolved with a 2 eV Gaussian broadening function.[a] Fitting range: 5700–5745 eV

	Lorentzian				Arctangent		
	A	H	W	E	H	W	E
Ce_2MoO_6	18.9	2.23	5.4	5722.2	0.89	0.1	5718.1
$Ce^{III}TiO_3$	18.9	2.44	4.9	5721.7	0.87	0.1	5718.2
$Ce^{III}(NO_3)_3 \cdot nH_2O$	21.2	3.97	3.4	5721.7	0.78	0.6	5718.9
$Ce_2^{III}(C_2O_4)_3 \cdot nH_2O$	22.3	3.99	3.6	5722.0	0.76	0.1	5719.1
$Ce^{IV}O_2$	11.6	1.13	6.5	5725.7	0.79	1.3	5720.0
	9.7	1.00	6.1	5733.4			

[a]See F.W. Lytle, R.B. Greegor and E.C. Marques, in M.J. Phillips and M. Ternan (eds.), *Proc. 9th Int. Congress on Catalysis*, Calgary, Vol. 5, The Chemical Institute of Canada, Ottawa, 1988, p. 54; and G. Krill, *J. Phys., 47 Coll., C8* (1986) C8-907.

longer (>0.1 Å) than the Ce–O distance for $Ce^{IV}O_2$ (2.343 Å [19]).

3.4. Valence considerations

Our cerium L-edge XANES and EXAFS indicate that, to the level of sensitivity of the XAFS technique, Ce is trivalent in Ce_2MoO_6. This result rules out previously suggested distributions of cerium and molybdenum valences, such as $Ce^{III}Ce^{IV}Mo^{V}O_6$ and $Ce_2^{IV}Mo^{IV}O_6$ [3,4]. A $Ce_2^{III}Mo^{VI}O_6$ valence distribution makes it difficult to rationalize the structural and physical properties of Ce_2MoO_6 with respect to those for the other rare earth molybdates in the $RE_2^{III}MoO_6$ series. As previously mentioned, Ce_2MoO_6 is unusual for two reasons: (1) it is the only member of the series that appears to crystallize in the cubic *Fm3m* space group; and (2) it is the only member of the series that does not assume the color of the rare earth ion but is, instead, black. It has been suggested that the color is due to molybdenum in a reduced oxidation state, *i.e.* Mo^{V} [3,4]. This suggestion has some experimental support from Mo K-edge XANES as well as EPR measurements [5]. The presence of Mo^{V} is not inconsistent with our result if it is assumed that the sample has a hypostoichiometric oxygen content, *i.e.* $Ce_2MoO_{6-\delta}$. This departure from stoichiometry would be rather surprising because in the series of rare earth molybdates with the composition RE_2MoO_5 ($\delta = 1.0$) for RE ≡ La–Ho, the cerium phase Ce_2MoO_5 does not form [20]. A slight oxygen deficiency may be sufficient to impart the unique color to Ce_2MoO_6

Because cerium is not quadrivalent in Ce_2MoO_6, it remains difficult to understand why it should behave differently from the other RE_2MoO_6 compounds. Our results suggest that the observed differences may be due to more subtle effects than those previously suggested [4,5].

4. Conclusion

Contrary to previous reports [3–5], the results of these Ce L-edge XAFS measurements reveal that Ce_2MoO_6 does not contain a mixed-valence distribution of trivalent and quadrivalent cerium, *i.e.* $Ce^{III}Ce^{IV}$-$Mo^{V}O_6$. Rather, the oxidation state of Ce was determined to be trivalent. The collection and analysis of high resolution Mo L-edge XANES (*ca.* 2500–2900 eV) are expected to provide direct insights about the oxidation state and site symmetry of Mo in Ce_2MoO_6.

Acknowledgments

We thank F.W. Lytle and S.R. Wasserman (ANL) for assistance with the XAFS measurements on X-23A2 at the NSLS, which is supported by the US Department Of Energy, Division of Material Sciences and Division of Chemical Sciences. This work was supported by the US DOE, Basic Energy Sciences–Chemical Sciences, under contract No. W-31-109-ENG-38.

References

1 A.V. Tyulin and V.A. Efremov, *Sov. Phys. Crystallogr., 32* (1987) 210.
2 P.V. Klevtsov, L.Yu. Kharchenko and R.F. Klevtsova, *Sov. Phys. Crystallogr., 20* (1975) 349.
3 L.H. Brixner, *Rev. Chim. Miner., 10* (1973) 47.
4 L.H. Brixner, A.W. Sleight and M.S. Licis, *J. Solid State Chem., 5* (1972) 186.
5 A. Manthiram and J. Gopalakrishnan, *J. Less-Common Met., 99* (1984) 107.
6 F.W. Lytle, in H. Winick, D. Xian, M.H. Ye and T. Huang (eds.), *Applications of Synchrotron Radiation*, Vol. 4, Gordon and Breach, New York, 1989, p. 135.
7 M.O. Krause and J.H. Oliver, *J. Phys. Chem. Ref. Data, 8* (1979) 329.

8 M.R. Antonio, in C.R. Brundle, C.A. Evans, Jr. and S. Wilson (eds.), *Encyclopedia of Materials Characterization: Surfaces, Interfaces, Thin Films*, Butterworth-Heinemann, Boston, 1992, p. 214.
9 (a) O. Muller and R. Roy, *Mater. Res. Bull., 4* (1969) 349. (b) H. Kerner-Czeskleba and G. Tourne, *Mater. Res. Bull., 13* (1978) 271.
10 S.P. Cramer, T.K. Eccles, F.W. Kutzler, K.O. Hodgson and L.E. Mortenson, *J. Am. Chem. Soc., 98* (1976) 1287.
11 A. Manthiram, P.R. Sarode, W.H. Madhusudan, J. Gopalakrishnan and C.N.R. Rao, *J. Phys. Chem., 84* (1980) 2200.
12 G.N. George, W.E. Cleland, Jr., J.H. Enemark, B.E. Smith, C.A. Kipke, S.A. Roberts and S.P. Cramer, *J. Am. Chem. Soc., 112* (1990) 2541.
13 J.E. Sunstrom, IV, S.M. Kauzlarich and M.R. Antonio, *Chem. Mater., 5* (1993) 182.
14 M.R. Antonio, J.F. Brazdil, L.C. Glaeser, M. Mehicic and R.G. Teller, *J. Phys. Chem., 92* (1988) 2338.
15 F. Le Normand, L. Hilaire, K. Kili, G. Krill and G. Maire, *J. Phys. Chem., 92* (1988) 2561.
16 (a) A.J. Davenport, H.S. Isaacs and M.W. Kendig, *Corrosion Sci., 32* (1991) 653. (b) A. Marcelli and A. Bianconi, *Physica B, 158* (1989) 529.
17 A. Santoro, M. Marezio, R.S. Roth and D. Minor, *J. Solid State Chem., 35* (1980) 167.
18 H. Barnighausen and G. Schiller, *J. Less-Common Met., 110* (1985) 385.
19 H.J. Whitfield, D. Roman and A.R. Palmer, *J. Inorg. Nucl. Chem., 28* (1966) 2817.
20 A. Manthiram and J. Gopalakrishnan, *J. Less-Common Met., 68* (1979) 167.